International Journal of Pharmaceutics 419 (2011) 287–295

Contents lists available at ScienceDirect

International Journal of Pharmaceutics

journal homepage: www.elsevier.com/locate/ijpharm

Pharmaceutical Nanotechnology

Lipid nanoparticles for brain targeting I. Formulation optimization

Paolo Blasi[a,*], Stefano Giovagnoli[a], Aurélie Schoubben[a], Carmelo Puglia[b], Francesco Bonina[b], Carlo Rossi[a], Maurizio Ricci[a]

[a] Dipartimento di Chimica e Tecnologia del Farmaco, Università degli Studi di Perugia, via del Liceo 1, 06123 Perugia, Italy
[b] Dipartimento di Scienze Farmaceutiche, Università degli Studi di Catania, viale A. Doria 6, 95125 Catania, Italy

ARTICLE INFO

Article history:
Received 3 March 2011
Received in revised form 20 July 2011
Accepted 22 July 2011
Available online 28 July 2011

Keywords:
Lipid nanoparticles
Colloids
Blood–brain barrier
Neurovascular unit
Brain targeting
Response surface methodology

ABSTRACT

The aim of this study was to optimize the formulation of lipid nanoparticles (NPs), intended for brain targeting, with the aid of a computer generated experimental design. The high pressure homogenization technique, selected for this purpose, was suitable to formulate the 3 investigated lipids (i.e., Softisan® 142, SOFT; Compritol® 888 ATO, COMP; cetyl palmitate, CP) into nanometre-length particles, while the computer generated experimental design helped to individuate the best preparation conditions with a small number of experimental assay. Even though all the 3 optimized formulations were suitable for intravenous infusion, CP NPs showed the smallest particle size and the appropriate thermal behaviour to be used as carriers in brain targeting applications.

1. Introduction

Nowadays, brain drug development still remains a challenging task due to the presence of the blood–brain barrier (BBB), a very restrictive barrier mainly composed of tightly sealed endothelial cells (Su and Sinko, 2006). In fact, due to its anatomy and physiology, the BBB strictly regulates the brain access and clearance of endogenous and exogenous molecules from the systemic circulation (Cornford and Hyman, 1999; Ballabh et al., 2004). BBB development and maintenance are possible because of the complex interactions between neurons, astrocytes, pericytes and microglia. This ensemble forms the so-called neurovascular unit (Neuwelt, 2004).

It is estimated that more than 98% of the new discovered central nervous system (CNS) potential drugs does not cross the BBB, failing to achieve therapeutic concentration within the brain parenchyma (Pardridge, 2001).

During the last three decades, different approaches have been developed to circumvent the BBB (Ricci et al., 2006; Neuwelt et al., 2008). Among others, embedding drugs within nanoparticulate matter able to cross the BBB is considered one of the most promising (Ricci et al., 2006; Celia et al., 2010). In particular, the possibility to tailor the nanoparticle (NP) surface to target specific tissues or organs is very attracting. Polymeric NPs decorated with opioid peptides or monoclonal antibodies have demonstrated interesting potentialities as carriers for brain drug targeting (Tosi et al., 2008; Aktas et al., 2005). A further attractive approach is based on the modification of the NP surface with specific surfactants able to adsorb preferentially apolipoproteins (Apo) from the blood stream (Göppert and Müller, 2003; Tröster et al., 1992). The Apo adsorbed on the surface, by interacting with specific receptors on the BBB luminal face, seems to be responsible for NP translocation into the brain (Kreuter, 2005). This mechanism has been recently corroborated through the observation that Apo-E coated albumin NPs are delivered in different brain regions (i.e., olfactory bulb, cortex, striatum, hippocampus, cerebellum, and the brain stem) 15 and 30 min after intravenous injection (Zensi et al., 2009). Similar promising results were obtained using lipid NPs stabilized with the same surfactants (Podio et al., 2000; Koziara et al., 2004; Blasi et al., 2009).

In this regards, lipids and waxes, due to their low toxicity and high biocompatibility (Souto et al., 2009), present some potential advantages over synthetic polymers for the preparation of NPs (Blasi et al., 2007; Kaur et al., 2008; Müller et al., 1996, 1997). In fact, lipid NPs, also referred as solid lipid nanoparticles (SLN) or nanostructured lipid carriers (NLC), have been virtually proposed for all administration routes, e.g., parenteral (Müller et al., 2004), oral (Zara et al., 2002), dermal (Puglia et al., 2008), and ocular

Abbreviations: Apo, apolipoproteins; BBB, blood–brain barrier; CNS, central nervous system; CP, cetyl palmitate; COMP, Compritol® 888 ATO; DSC, differential scanning calorimetry; GDW, Gaussian distribution width; MHD, mean hydrodynamic diameter; NP, nanoparticle; NPs, snanoparticles; NLC, nanostructured lipid carriers; PCS, photo correlation spectroscopy; P80, polysorbate 80; SOFT, Softisan® 142; SLN, solid lipid nanoparticles; TEM, transmission electron microscopy.

* Corresponding author. Tel.: +39 0755852057; fax: +39 0755855163.
E-mail address: kaolino@unipg.it (P. Blasi).

0378-5173/$ – see front matter © 2011 Elsevier B.V. All rights reserved.
doi:10.1016/j.ijpharm.2011.07.035

(Cavalli et al., 2002). SLN and NLC refer to colloids produced by lipids, namely fatty acids, mono-, di-, and tri-glycerides, waxes and nonsaponificable lipids, solid at the body temperature. SLN are generally prepared with one or a mixture of solid lipid materials, while NLC are composed of a solid lipid and a certain amount of liquid lipid (oil), maintaining the solid state at both room and body temperature. NLC have been developed as an evolution of SLN. In fact, the presence of a certain amount of oil reduces the tendency of the matrix to crystallize with many advantages for the system, such as increased drug loading and retention (squeezing reduction), enhanced physical stability, and improved controlled release (Saupe et al., 2005).

Unfortunately, the fabrication of stable materials at nanometre-length scale is difficult and most of the proposed methods are exploitable only at the laboratory scale (Blasi et al., 2007; Müller and Runge, 1998). However, the use of high pressure homogenization may overcome such inconveniences due to reproducibility and scale-up possibility (Müller et al., 2004). In fact, homogenizers have been used in the food industry for more than a century to process highly fat products (Pandolfe, 1982).

Following such considerations, this work is aimed at optimizing the preparation of lipid NPs for brain drug targeting. For this purpose, a response surface methodology was employed to assess the conditions leading to best particle features. Lipid NPs were characterized for their size (i.e., mean diameter and polydispersity), morphology, and thermal behaviour. Due to the particular importance of particle size in brain drug delivery (Gao and Jiang, 2006), the target NP formulation was chosen as function of particle size as well as milder working conditions.

2. Materials and methods

2.1. Materials

COMP, a mixture of mono-, di- and triglycerides of behenic acid, also known as glyceryl behenate or tribehenin, and CP were kind gifts of Gattefossé (Milan, Italy). SOFT (hydrogenated coco glycerides), a mixture of hydrogenated vegetable fatty acids with a chain length of 10–18 carbon atoms, was kindly provided by Eigenmann & Veronelli (Milan, Italy).

Polysorbate 80 (HX)^{TM} (P80) of injectable grade was a kind gift of NOF corporation (Tokyo, Japan). Ultra pure water (ρ, 18.2 MΩ cm) was obtained by a Milli-Q system (Millipore, Rome, Italy). All other materials were of analytical grade and used as provided.

2.2. Preparation of lipid nanoparticles

Lipid NPs were prepared using the hot high pressure homogenization technique as reported elsewhere (Blasi et al., 2009). Briefly, 5 g of the chosen lipid were heated up to a temperature 10 °C above its melting point (SOFT, m.p. ~ 42 °C; CP, m.p. ~ 55 °C; COMP, m.p. ~ 70 °C) and added drop wise to 35 mL of a P80 aqueous solution under high-speed stirring (1 min, 8000 rpm; Ultra Turrax T25, IKA® Werke GmbH & Co. KG, Staufen, Germany), to prepare an emulsion. Surfactant solution was thermostated at the same temperature of the molten lipid (i.e., 10 °C > m.p. for COMP and CP, 10 and 20 °C > m.p. for SOFT) and the addition rate was 2.5 g/min. The obtained pre-emulsion was then processed with a high pressure homogenizer (Avestin EmulsiFlex-C5, Ottawa, Canada) at the same temperatures and at a pressure of 1500 bar. Only in the case of SOFT, two different homogenization temperatures were investigated: at 10 and 20 °C above the melting point. After homogenization, the hot dispersion was immediately cooled in an ice bath obtaining solid lipid NPs.

Table 1
Fabrication parameters studied to build the models.

Matrices	P80 concentration (% w/v), X_B	Homogenization cycles (number), X_A	Temperature (°C), X_C
Compritol® 888 ATO	0.5	1–10	80
	1	1–10	
	1.5	1–10	
	2	1–10	
Softisan® 142	0.5	1–10	52
	1	1–10	
	1.5	1–10	
	2	1–10	
	0.5	1–10	62
	1	1–10	
	1.5	1–10	
	2	1–10	
Cetyl palmitate	0.50	1, 5, 10	65
	0.88	3, 8	
	1	1, 10	
	1.25	5	
	1.50	1, 10	
	2	1, 5, 10	

2.3. Factorial design study

A computer generated experimental design was built to evaluate the effects of the preparation factors on the mean hydrodynamic diameter (MHD) and Gaussian distribution width (GDW) of lipid NP formulations. Factors were selected according to the parameters characterizing the hot melt homogenization method as well as to the results of preliminary experiments. When COMP and CP were employed, the number of homogenization cycles (X_A) and surfactant concentration (X_B) were considered the main factors affecting particle size and distribution. In the case of SOFT, the homogenization temperature (X_C) was included as third factor. Conditions were varied as described in Table 1. Three replicates per batch were performed in order to assess process and system reproducibility. The complete general polynomial regression model chosen is described by the following equation:

$$Y = \beta_0 + \beta_1 X_A + \beta_2 X_B + \beta_3 X_C + \beta_4 X_A X_B + \beta_5 X_A X_C + \beta_6 X_B X_C + \beta_7 X_A^2 + \beta_8 X_B^2 + \beta_9 X_C^2 + \beta_{10} X_A X_B X_C + \beta_{11} X_A^2 X_B + \beta_{12} X_A^2 X_C + \beta_{13} X_B^2 X_A + \beta_{14} X_B^2 X_C + \beta_{15} X_C^2 X_A + \beta_{16} X_C^2 X_B + \beta_{17} X_A^3 + \beta_{18} X_B^3 + \beta_{19} X_C^3 + \cdots + \varepsilon \quad (1)$$

where Y is the dependent variable, and β_i the multiple regression coefficients representing estimates of main effects and interactions. In particular, β_1–β_3 represents main effects, β_4–β_9 two-factor interactions, and β_{10}–β_{19} three-factor interactions. X_A, X_B, X_C are the three investigated factors and ε the residual error of the model.

Eq. (1) was applied to different lipid NP formulations and evaluated in term of statistical significance by ANOVA. In addition, the possible presence of multicollinearity, outliers and lack of fit were estimated. Contour plots displaying MHD and GDW behaviours at different X_A and X_B levels were built. In the case of SOFT, two plots related to low (52 °C) and high (62 °C) X_C factor levels were drawn. Statistical and factorial analyses were performed by using Design-Expert® v. 8.0.1 (Stat-Ease Inc., Minneapolis, MN, USA).

2.4. Optimality region assessment

A response surface methodology was used to plot response behaviour against factor levels. The contour plots, obtained from model regression to the experimental points for MHD and GDW, were investigated to assess the optimality region. For this purpose, the desirability function approach was applied to the system in

Table 2
Predicted and experimental MHD and GDW values for the 3 models.

Number of cycles	P80 concentration (%, w/v)	Actual MHD (nm) ± S.D.	Predicted MHD (nm)	Bias (%)	Actual GDW (nm) ± S.D.	Predicted GDW (nm)	Bias (%)
Softisan							
$T = 52\,^{\circ}C$							
3	1.0	222.5 ± 6.6	254.2	12.5	127.2 ± 10.5	129.2	1.5
6		259.0 ± 68.1	226.4	12.6	150.8 ± 68.9	125.6	16.7
3	1.5	229.9 ± 4.4	267.9	14.2	119.4 ± 3.7	147.5	19.1
6		243.3 ± 5.6	267.9	9.2	128.0 ± 9.0	147.5	13.2
$T = 62\,^{\circ}C$							
3	1.0	272.9 ± 33.9	272.7	0.07	134.6 ± 12.7	129.2	4.0
6		262.0 ± 47.7	270.2	3.0	134.5 ± 25.2	125.7	6.5
3	1.5	282.8 ± 46.8	312.0	9.4	124.1 ± 10.8	147.5	15.9
6		284.1 ± 46.1	309.6	8.2	125.8 ± 14.9	143.1	12.1
Compritol							
4	1.0	311.6 ± 27.3	296.8	4.7	146.1 ± 7.6	144.7	1.0
7		286.8 ± 16.7	291.5	1.6	121.0 ± 24.7	155.9	22.4
4	1.5	341.1 ± 28.3	389.3	12.4	175.7 ± 4.7	171.1	2.6
7		424.4 ± 28.0	383.3	9.6	193.7 ± 12.8	185.6	4.2
Cetyl palmitate							
1	0.88	328.1 ± 7.3	306.6	6.6	117.6 ± 13.8	112.9	4.2
10		283.2 ± 7.0	277.3	2.1	103.3 ± 5.4	98.7	4.5
1	1.25	293.3 ± 10.6	281.7	4.0	95.5 ± 15.5	101.2	5.6
10		258.7 ± 15.2	251.5	2.8	85.4 ± 10.9	89.1	4.2

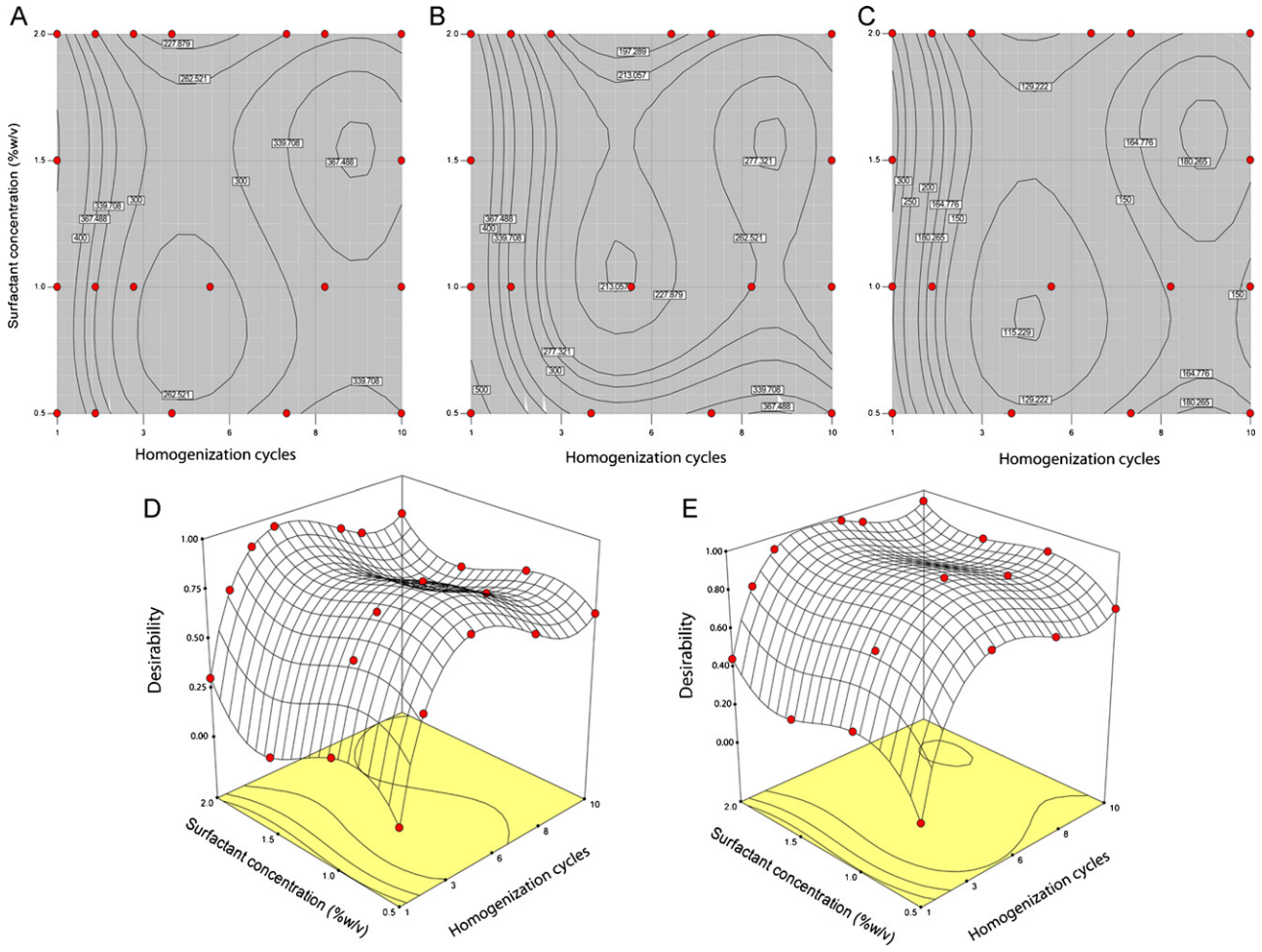

Fig. 1. Contour plots of Softisan® 142 NPs showing the effect of homogenization cycles (1–10) and surfactant concentration (0–2%, w/v) at 55 °C on MHD (A) and GDW (C) as well as at 65 °C on MHD (B). Response surface plot showing the desirability at 55 (D) and 65 °C (E).

Table 3
Predictivity outside the model working area for SOFT.

Number of cycles	P80 concentration (%, w/v)	Experimental MHD (nm) ± S.D.	Predicted MHD (nm)	Bias (%)	Experimental GDW (nm) ± S.D.	Predicted GDW (nm)	Bias (%)
5	2.5	164.7 ± 6.5	173.6	5.4	93.3 ± 15.4	108.7	16.5
5	3	160.0 ± 20.9	157.6	1.5	89.5 ± 11.0	104.4	16.7
5	3.5	151.4 ± 18.2	144.2	4.8	82.3 ± 5.7	100.4	22.0
5	4	151.1 ± 10.1	133.0	12.0	86.1 ± 7.1	96.6	12.2

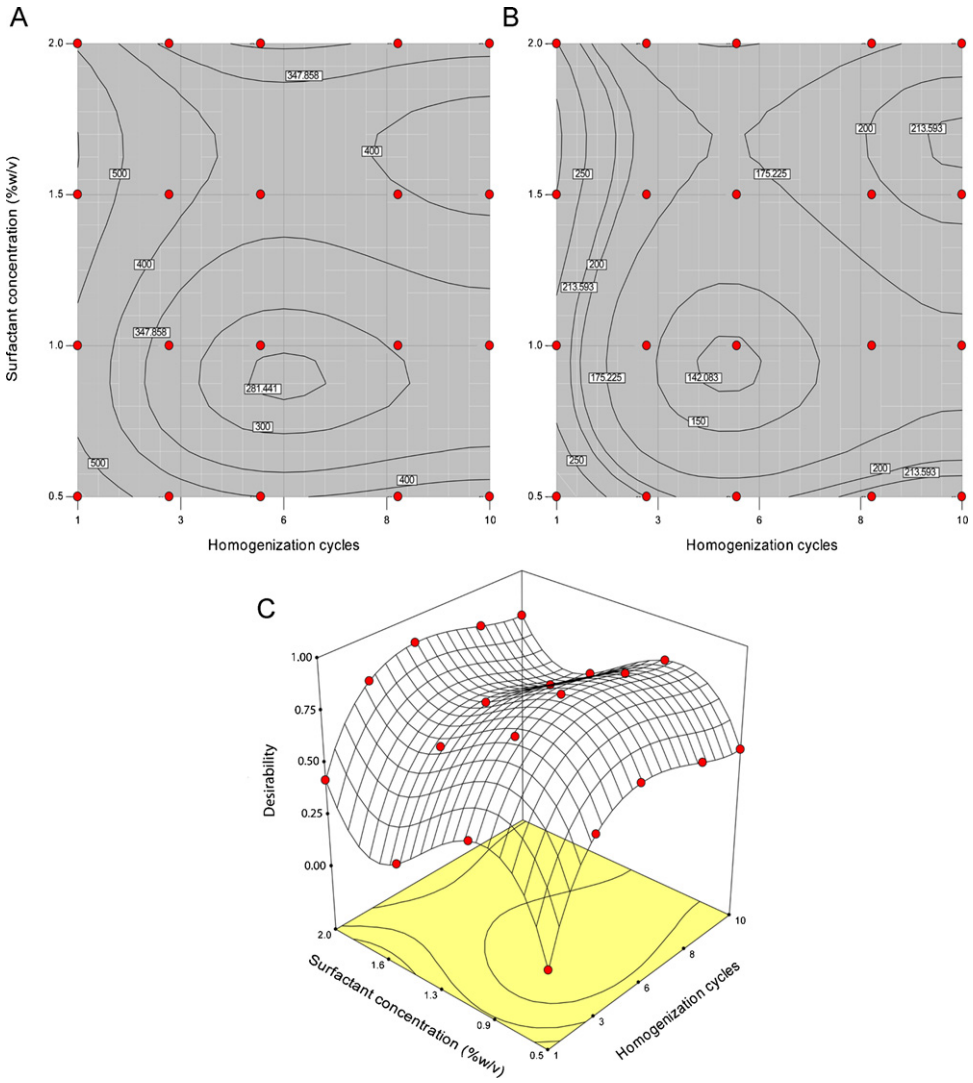

Fig. 2. Contour plots of Compritol® 888 ATO NPs showing the effect of homogenization cycles (1–10) and surfactant concentration (0–2%, w/v) on MHD (A) and GDW (B). Response surface plot showing the desirability (C).

order to delimit the region corresponding to the smallest MHD and GDW (Eq. (2)).

$$D = (d_1 d_2 \dots d_m)\frac{1}{m} \quad (2)$$

where m is the response and d is the individual desirability functions for each response, namely the smallest MHD as well as GDW.

2.5. Check-point analysis

Check-point analyses were carried out to establish model reliability. Series of points were chosen according to the obtained contour plots and all experiments were performed in triplicate. Bias was estimated to evaluate the agreement between actual and predicted values. Further experiments were carried out in the case the region of higher desirability stretched outside the working frame.

2.6. Particle size distribution and morphology

Lipid NP size was measured by photo correlation spectroscopy (PCS) and expressed as MHD and GDW. Dimensional distribution analyses were performed using a Nicomp 380 autocorrelator (PSS Inc., Santa Barbara, CA, USA) equipped with a Coherent Innova 70-3 (Laser Innovation, Moorpark, CA, USA) argon ion laser.

LNs were morphologically characterized by means of transmission electron microscopy (TEM) (Philips EM 400T microscope, Eindhoven, Nederlands). Samples were prepared by simply depositing a drop of the NP suspension on the surface of a 200

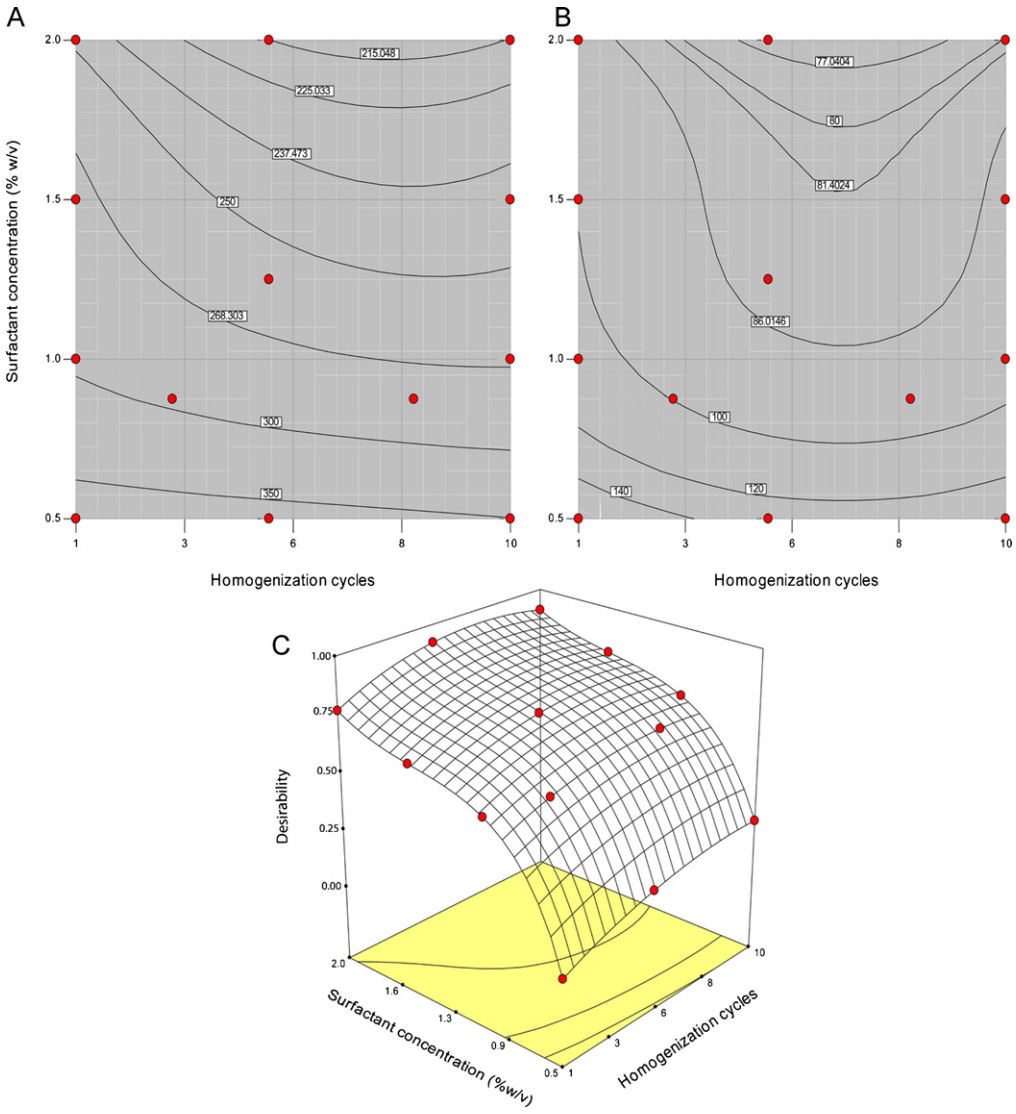

Fig. 3. Contour plots of cetyl palmitate NPs showing the effect of homogenization cycles (1–10) and surfactant concentration (0–2%, w/v) on MHD (A) and GDW (B). Response surface plot showing the desirability (C).

mesh Formvar® coated copper grid (TAAB Laboratories Equipment Ltd., Aldermaston, England) and letting it to dry overnight.

2.7. Differential scanning calorimetry

Differential scanning calorimetry (DSC) was performed to characterize lipid NP thermal behaviour. Experiments were run by using a DSC821e (Mettler Toledo, Greifensee, Switzerland) calorimeter, equipped with a liquid nitrogen cooling system. A nitrogen purge at a flow rate of 50 cm^3/min was used to provide an inert gas atmosphere in the DSC cell. The system was calibrated using an indium standard with a hermetic sealed empty pan as reference. Prior to heating, samples were equilibrated in a hermetic sealed 40 μL aluminum pan at 20 °C for 10 min. In all cases, heating or cooling rate of 10 °C/min was used. Data were treated with STARe software (Mettler Toledo International Inc., Greifensee, Switzerland) and the results expressed as the mean of two determinations.

3. Results and discussion

3.1. Nanoparticle preparation

The hot high pressure homogenization technique was able to produce nano-scale particles, regardless the employed matrix material (i.e., COMP, SOFT, and CP). From preliminary experiments, the surfactant concentration and the number of homogenization cycles resulted the most significant fabrication parameters. In fact, even though homogenization pressure has a fundamental importance in drop breakage and the achievement of a small particle size (Narsimhan and Goel, 2001), in previous experiments, to obtain a narrow droplet/particle size distribution, a pressure of at 1000 bar was needed (Puglia et al., 2008). Obviously, this is strictly related to the intrinsic characteristics of the instrument (e.g., homogenizer valve type and design, single-piston, multi-pistons) and different homogenizers might also need lower pressures to obtain similar results (Müller et al., 2004). With the present experimental setup, preliminary homogenization experiments at different pressures showed the need of 1500 bar to obtain low particle size and polydispersity. Then, the computer generated experimental design helped establishing the optimal value combination of the abovementioned factors (Dhawan et al., 2011). Nonlinear models were validated by ANOVA and the results (MHD and GDW), expressed as contour and surface response plots, are reported and discussed separately for the three starting materials.

Three lipids having different nature and structure, two triglyceride mixtures with different carboxylic acid chain length (i.e., SOFT and COMP) and a wax (i.e., CP), were selected and used to

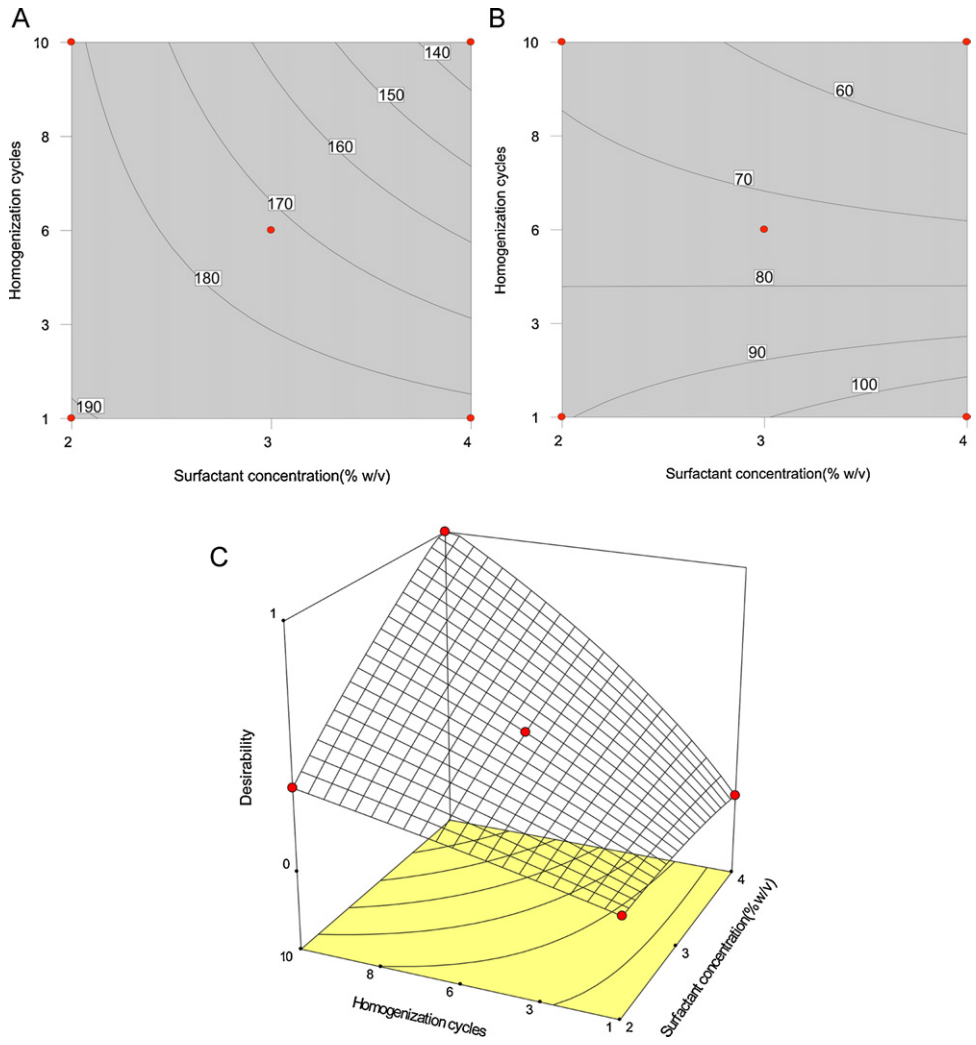

Fig. 4. Contour plots of cetyl palmitate NPs showing the effect of homogenization cycles (1–10) and surfactant concentration (2–4%, w/v) on MHD (A) and GDW (B). Response surface plot showing the desirability (C).

produce NPs. Due to the P80 peculiar role in brain drug targeting, the evaluation of the effect of different surfactants was considered unnecessary and rather the effect on particle size of surfactant concentration was accounted together with the number of homogenization cycles. The effect of the homogenization temperature was investigated only in the case of SOFT to establish the possibility to reduce particle size increasing temperature since the low lipid melting temperature allowed to investigate working temperatures 10 and 20 °C higher than the melting one.

3.1.1. *Softisan® 142 nanoparticles*

As anticipated, in the case of SOFT NPs, the number of homogenization cycles (X_A), surfactant concentration (X_B), and the homogenization temperatures (X_C) were considered the main factors affecting particle size and distribution. Eqs. (3) and (4) represent the obtained nonlinear models resulting from ANOVA calculations.

$$\mathrm{MHD} = 250.8 + 81.9A + 51.3\,B + 29.3C - 0.1AB + 19.0AC + 19.2BC + 130.9A^2 + 2.8B^2 - 28.0B^2C - 179.1\,A^3 - 103.7B^3 \quad (3)$$

$$\mathrm{GDW} = 0.088 - 0.015A - 0.0099B + 0.00068AB - 0.021A^2 + 0.00043B^2 + 0.028A^3 + 0.014B^3 \quad (4)$$

The high significance of the model ($P < 0.0001$) can be confirmed by the coefficient of variance values (MHD, 9.17; GDW, 9.89) and the correlation coefficients ($r^2 = 0.9164$; 0.7515). Moreover, the analysis of the response surfaces showed a nonsignificant lack-of-fit (data not shown).

According to Eqs. (3) and (4), homogenization cycles (X_A), surfactant concentration (X_B) and the preparation temperature (X_C) have a determinant effect on the MHD, whereas X_C seems to be marginal for GWD. In both cases, the number of cycles shows the strongest effect.

Fig. 1A–C describe the effect of X_A, X_B and X_C on MHD and GDW, while Fig. 1D and E shows the desirability plots obtained combining the individual response surfaces for MHD and GDW. To confirm the regression model predictivity, check point analysis at 1 and 1.5% (w/v) P80 concentrations and at 3 and 6 homogenization cycles was performed. As it can be observed in Table 2, the model predictivity was satisfactory. The preparations performed at 62 °C were also in good agreement with model predictions, but the best working temperature was found to be 52 °C (Table 2). In fact, while higher temperatures generally correspond to a lower melt viscosity and to higher homogenizer performance, in this specific case an opposite effect was observed. This could be due to the formation of very fine droplets with a short life span due to the increased chance of aggregation and coalescence. This effect is linked to the concomitant high shear, cavitational forces and surface area increase.

Table 4
Predictivity outside the model working area for CP.

Check points		Predicted values		Actual values		Bias mean size (%)	Bias distribution width (%)
Number of homogenization cycles	Surfactant concentration (%, w/v)	Mean size (nm)	Distribution width (nm)	Mean size (nm) ± S.D.	Distribution width (nm) ± S.D.		
7	2	184.6	72.9	189.7 ± 4.4	74.3 ± 2.4	−2.8	−1.9
7	3	167.4	67.9	163.8 ± 6.5	63.8 ± 1.1	2.1	5.9
7	4	150.2	63.5	138.6 ± 4.4	56.1 ± 5.1	7.7	11.7

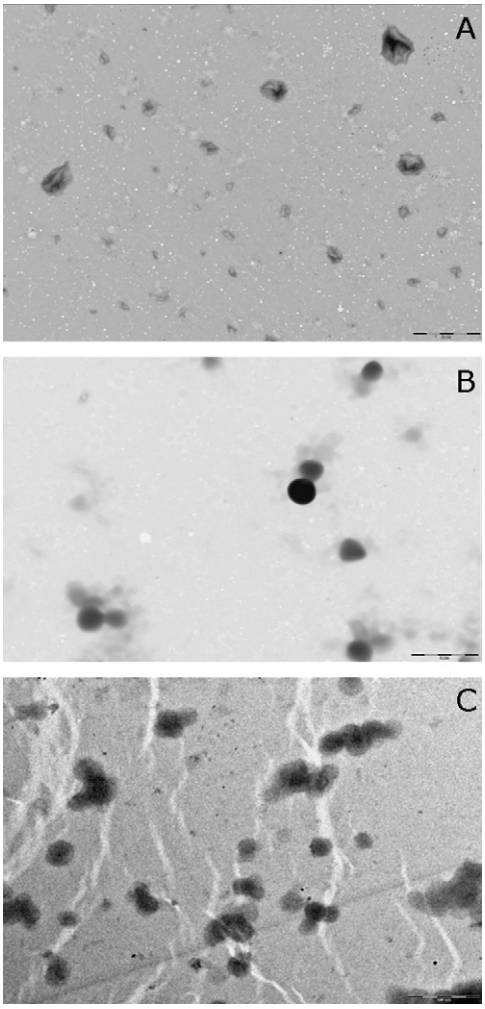

Fig. 5. Transmission electron microscopy of Softisan® 142 (A), Compritol® 888 ATO (B) and cetyl palmitate (C) NPs.

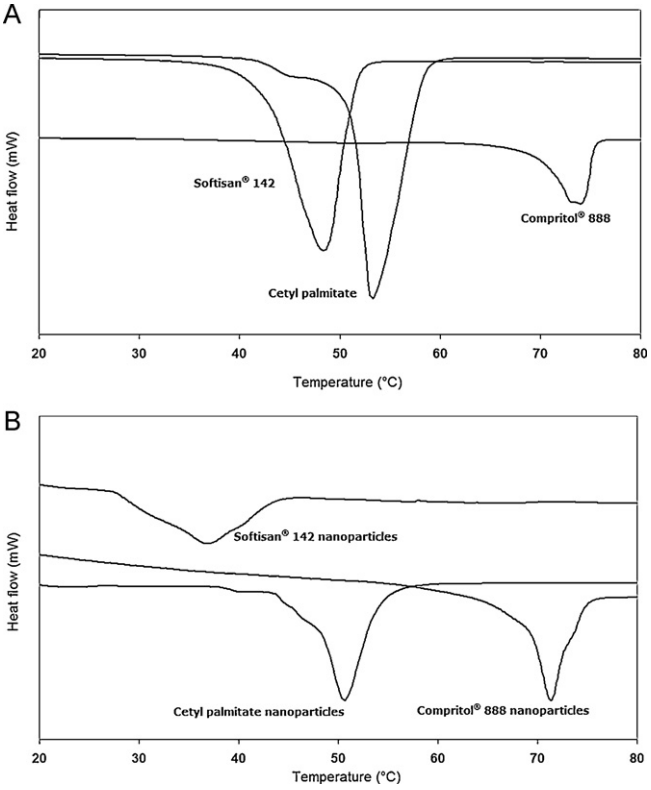

Fig. 6. DSC data of the bulk (A) and colloidal (B) lipid materials.

According to the contour plots, there is a decrease of size and size dispersion towards P80 concentrations higher then 2%. Such trend seems to suggest a further lowering of both MHD and GDW well beyond the 2% value. This hypothesis was verified by performing studies at 2.5, 3, 3.5, and 4% (w/v) of P80 concentrations (5 homogenization cycles at 52 °C). In fact, the MHD and GDW were reduced and resulted minimum at 3.5% (w/v) with the highest agreement between the predicted and the experimental values as well (Table 3).

3.1.2. Compritol® 888 nanoparticles

The second lipid matrix investigated, COMP, a mixture of mono-, di- and triglycerides of behenic acid, has been extensively employed as excipient for controlled release purpose (Brubach et al., 2007). In addition, it has been largely used for the production of SLN and NLC (Souto et al., 2006; Hamdani et al., 2003).

With COMP, only the influence of the homogenization cycles (X_A) and surfactant concentration (X_B) was investigated due to the higher melting point of the lipid. Eqs. (5) and (6) represent the non-linear models obtained to describe the behaviour of MHD and GDW, respectively.

$$\mathrm{MHD} = 18.02 - 0.013A + 4.40B + 2.96A^2 + 0.50B^2 - 1.97A^3 - 5.84B^3 \quad (5)$$

$$\mathrm{GDW} = 0.081 - 0.0048A - 0.013B - 0.013A^2 - 0.0039B^2 + 0.011A^3 + 0.018B^3 \quad (6)$$

It is evident from Eqs. (5) and (6) that the surfactant concentration had a stronger influence on MHD and GDW than the number of cycles.

ANOVA and the statistic validation reported a high significance of the mathematical models ($P < 0.0001$), confirmed also by the coefficient of variance values (MHD, 4.20; GDW, 6.13) and the correlation coefficients ($r^2 = 0.8775$; 0.7621). Besides, there was a not significant lack-of-fit for both MHD and GDW (data not shown).

Moreover, the presence of nonsignificant A and B^2 terms for MHD and A term for GDW demonstrated that homogenization cycles (X_A) by themselves had a minor influence on the responses, whereas a strong effect when combined with the other factors.

Table 2 displays the theoretical and predicted values of MHD and GDW. The check points were evaluated at two concentrations: 1 and 1.5% (w/v), and at 4 and 7 homogenization cycles, respectively. The predicted and the observed values were in good agreement with biases well below 13% for most of the evaluated model points (Table 2).

Modelling of response behaviour against the factor levels was accomplished by using contour and response surface plots. Fig. 2A and B display the effect of the homogenization cycles (X_A) and surfactant concentration (X_B) on the responses, while Fig. 2C shows the resulting desirability plot, which framed the optimal production conditions at 5 homogenization cycles and a P80 concentration of 0.91% (w/v).

3.1.3. Cetyl palmitate nanoparticles

As in the previous case (i.e., COMP NPs), the influence of the homogenization cycles (X_A) and surfactant concentration (X_B) were investigated being these the most determinant parameters. Eqs. (7) and (8) represent the nonlinear models obtained to describe the behaviour of MHD and GDW against X_A and X_B.

$$\mathrm{MHD} = 0.063 + 0.0017A + 0.0049B + 0.00053AB - 0.0013A^2 - 0.0023B^2 - 0.0013A^2B + 0.0032B^3 \quad (7)$$

$$\mathrm{GDW} = 0.11 + 0.0033A + 0.0043B - 0.0068A^2 - 0.0082B^2 + 0.0095B^3 \quad (8)$$

The statistical validation by ANOVA showed a high significance of the model ($P < 0.0001$), confirmed also by the coefficient of variance values (MHD, 1.76; GDW, 5.70) and the correlation coefficients ($r^2 = 0.9622$; 0.7773). The analysis of the response surfaces indicated a nonsignificant lack-of-fit for both models (MHD and GDW) and the check-point analysis confirmed the good agreement between predicted and actual values, with bias lower than 7% (Table 2).

Even in this case, the desirability plot was built combining the effect of X_A and X_B on both MHD and GDW. The best conditions were found at 2% (w/v) of P80 and 7 homogenization cycles (Fig. 3C). However, the trend observed suggested a possible further improvement outside of the investigated working frame, in particular by using higher surfactant concentrations (Table 4).

While a number of homogenization cycle higher than 7 led to a substantial increase of particle size for SOFT and COMP, in the case of CP this effect, probably due to a shortage of P80, was negligible. When the surfactant concentration was increased, this behaviour disappeared (Fig. 4). This phenomenon is generally due to droplet size reduction generating a very large interface, not well stabilized by the surfactant. In fact, after parent droplet breakage in the valve, the newly formed droplets are stable only if enough surfactant is present to cover the larger interface and if the timescale of surfactant adsorption is smaller than that of coalescence (Narsimhan and Goel, 2001).

In the working frame consisting of 2–4% (w/v) of P80 and 1–10 homogenization cycles, MHD decreased proportionally to the increase of surfactant and homogenization cycles (Fig. 4A and B), leading to a maximum desirability when both parameters were maximum (P80, 4% (w/v); cycles; 10) (Fig. 4C). The mentioned preparation conditions led to a mean particle size lower than 140 nm and a very narrow Gaussian distribution (Fig. 4).

3.2. Nanoparticle characterization

As previously mentioned, all the obtained NPs were characterized by a nanometre size, even in the worst case conditions. This observation, together with the lack of organic solvents and the easy scalability, confirms the great potential of high pressure homogenization as a reliable technique for laboratory and industrial scale lipid NP preparation (Blasi et al., 2007; Müller et al., 2004).

However, as previously reported, the investigated parameters had a different influence on droplet size reduction and then on the final particle size. Differences observed on the influence of surfactant concentration and homogenization passes may be ascribed to the diverse chemical structure and main composition of the lipid materials, determining different hydrophobicity and viscosity (Yang et al., 2011; Triplett and Rathman, 2009).

In this regards, TEM analyses showed particle sizes compatible with those obtained by PCS in spite of the presence of some aggregates that were ascribed to the procedure employed for sample preparation (Fig. 5). NP morphology seemed changing according to the diverse matrices employed. In fact, while COMP and CP yielded spherical NP, SOFT produced wrinkled particles. This was likely due to artefacts produced by lipid melting and shrinking during the analysis because of the high energy of the electron beam that can provoke local heating in the lipid matrix (Baker and Holloway, 1971). This hypothesis was supported by the DSC analysis, which showed a melting point depletion below 37 °C for SOFT NPs compared to the bulk lipid (Fig. 6A).

This is a behaviour common to most lipid materials that undergo such melting temperature decrease when formulated as colloids (Fig. 6B) and is generally due to both the colloidal size and the presence of the surfactant (Bunjes and Unruh, 2007). This decrease is more consistent in the case of SOFT, leading to a melting temperature lower than 37 °C. This formulation should behave *in vivo* exactly as an emulsion and, therefore, should not be addressed as SLN. In the other 2 cases (i.e., COMP and CP) the melting temperature remained higher than the body temperature and therefore NPs will be still in a solid state after injection.

4. Conclusions

Lipid NPs were successfully formulated by hot high pressure homogenization using 3 different lipid matrixes and the effect of the main preparation parameters, namely surfactant concentration and number of homogenization cycles, was investigated. By using a computer generated experimental design and a response surface analysis it was possible to establish the best formulation conditions with a limited number of experiments.

From the obtained results it is possible to conclude that CP is a suitable lipid material to produce P80 coated NPs possessing particle sizes suitable for brain targeting by intravenous or intra-arterial injection.

Acknowledgments

The authors would like to thank Ewa Szymanowska for her help in the collection of the data.

References

Aktas, Y., Yemisci, M., Andrieux, K., Gursoy, R.N., Alonso, M.J., Fernandez-Megia, E., Novoa-Carballal, R., Quiñoa, E., Riguera, R., Sargon, M.F., Celik, H.H., Demir, A.S., Hýncal, A.A., Dalkara, T., Capan, Y., Couvreur, P., 2005. Development and brain delivery of chitosan-PEG nanoparticles functionalized with the monoclonal antibody OX26. Bioconjug. Chem. 16, 1503–1511.

Baker, E.A., Holloway, P.J., 1971. Scanning electron microscopy of waxes on plant surfaces. Micron 2, 364–380.

Ballabh, P., Braun, A., Nedergaard, M., 2004. The blood–brain barrier: an overview structure, regulation, and clinical implications. Neurobiol. Dis. 16, 1–13.

Blasi, P., Giovagnoli, S., Schoubben, A., Ricci, M., Rossi, C., 2007. Solid lipid nanoparticles for targeted brain drug delivery. Adv. Drug Deliv. Rev. 59, 454–477.
Blasi, P., Schoubben, A., Giovagnoli, S., Puglia, C., Barberini, L., Cirotto, C., Rossi, C., Ricci, M., 2009. Colloidal dispersions for targeted brain drug delivery. Eur. J. Pharm. Sci. 38S, 25–26.
Bunjes, H., Unruh, T., 2007. Characterization of lipid nanoparticles by differential scanning calorimetry, X-ray and neutron scattering. Adv. Drug Deliv. Rev. 59, 379–402.
Brubach, J.B., Jannin, V., Mahler, B., Bourgaux, C., Lessieur, P., Roy, P., Ollivon, M., 2007. Structural and thermal characterization of glyceryl behenate by X-ray diffraction coupled to differential calorimetry and infrared spectroscopy. Int. J. Pharm. 336, 248–256.
Cavalli, R., Gasco, M.R., Chetoni, P., Burgalassi, S., Saettone, M.F., 2002. Solid lipid nanoparticles (SLN) as ocular delivery system for tobramycin. Int. J. Pharm. 238, 241–245.
Celia, C., Cosco, D., Paolino, D., Fresta, M., 2010. Nanoparticulate devices for brain drug delivery. Med. Res. Rev., doi:10.1002/med.20201.
Cornford, E.M., Hyman, S., 1999. Blood–brain barrier permeability to small and large molecules. Adv. Drug Deliv. Rev. 36, 145–163.
Dhawan, S., Kapil, R., Singh, B., 2011. Formulation and development and systematic optimization of solid lipid nanoparticles of quercetin for improved brain delivery. J. Pharm. Pharmacol. 63, 342–351.
Gao, K., Jiang, X., 2006. Influence of particle size on transport of methotrexate across blood brain barrier by polysorbate 80-coated polybutylcyanoacrylate nanoparticles. Int. J. Pharm. 310, 213–219.
Göppert, T.M., Müller, R.H., 2003. Plasma protein adsorption of Tween® 80- and poloxamer 188-stabilized solid lipid nanoparticles. J. Drug Target. 11, 225–231.
Hamdani, J., Moës, A.J., Amighi, K., 2003. Physical and thermal characterisation of Precirol® and Compritol® as lipophilic glycerides used for the preparation of controlled-release matrix pellets. Int. J. Pharm. 260, 47–57.
Kaur, I.P., Bhandari, R., Bhandari, S., Kakkar, V., 2008. Potential of solid lipid nanoparticles in brain targeting. J. Control. Release 127, 97–109.
Koziara, J.M., Lockman, P.R., Allen, D.D., Mumper, R.J., 2004. Paclitaxel nanoparticles for the potential treatment of brain tumors. J. Control. Release 99, 259–269.
Kreuter, J., 2005. Application of nanoparticles for the delivery of drugs to the brain. Int. Congr. Ser. 1277, 85–94.
Müller, R.H., Maaβen, S., Weyhers, H., Specht, F., Lucks, J.S., 1996. Cytotoxicity of magnetide-loaded polylactide, polylactide/glycolide particles and solid lipid nanoparticles. Int. J. Pharm. 138, 85–94.
Müller, R.H., Radtke, M., Wissing, S.A., 2004. Solid lipid nanoparticles and nanostructured lipid carriers. In: Nalwa, H.S. (Ed.), Encyclopedia of Nanoscience and Nanotechnology. American Scientific Publishers, Los Angeles, pp. 43–56.
Müller, R.H., Rühl, D., Runge, S., Schulze-Forster, K., Mehnert, W., 1997. Cytotoxicity of solid lipid nanoparticles as a function of the lipid matrix and the surfactant. Pharm. Res. 14, 458–462.
Müller, R.H., Runge, S.A., 1998. Solid lipid nanoparticles (SLN®) for controlled drug delivery. In: Benita, S. (Ed.), Submicron Emulsions in Drug Targeting and Delivery. Harwood Academic Publishers, Amsterdam, pp. 219–234.
Narsimhan, G., Goel, P., 2001. Drop coalescence during emulsion formation in a high-pressure homogenizer for tetradecane-in-water emulsion stabilized by sodium dodecyl sulphate. J. Colloid Interface Sci. 238, 420–432.
Neuwelt, E.A., 2004. Mechanisms of disease: the blood–brain barrier. Neurosurgery 54, 131–140.
Neuwelt, E.A., Abbott, N.J., Abrey, L., Banks, W.A., Blakley, B., Davis, T., Engelhardt, B., Grammas, P., Nedergaard, M., Nutt, J., Pardridge, W., Rosenberg, G.A., Smith, Q., Drewes, L.R., 2008. Strategies to advance translational research into brain barriers. Lancet Neurol. 7, 84–96.
Pandolfe, W.D., 1982. Development of the new Gaulin micro-gap™ homogenizing valve. J. Dairy Sci. 65, 2035–2044.
Pardridge, W.M., 2001. Brain Drug Targeting: The Future of Brain Drug Development, first ed. Cambridge University Press, Cambridge.
Podio, V., Zara, G.P., Carazzone, M., Cavalli, R., Gasco, M.R., 2000. Biodistribution of stealth and non-stealth solid lipid nanospheres after intravenous administration to rats. J. Pharm. Pharmacol. 52, 1057–1063.
Puglia, C., Blasi, P., Rizza, L., Schoubben, A., Bonina, F., Rossi, C., Ricci, M., 2008. Lipid nanoparticles for prolonged topical delivery: an in vitro and in vivo investigation. Int. J. Pharm. 357, 295–304.
Ricci, M., Blasi, P., Giovagnoli, S., Rossi, C., 2006. Delivering drugs to the central nervous system: a medicinal chemistry or a pharmaceutical technology issue? Curr. Med. Chem. 13, 1757–1775.
Saupe, A., Wissing, S.A., Lenk, A., Schmidt, C., Müller, R.H., 2005. Solid Lipid Nanoparticles (SLN) and Nanostructured Lipid Carriers (NLC) – structural investigations on two different carrier systems. Biomed. Mater. Eng. 15, 393–402.
Souto, E.B., Mehnert, W., Müller, R.H., 2006. Polymorphic behaviour of Compritol®888 ATO as bulk lipid and as SLN and NLC. J. Microencapsul. 23, 417–433.
Souto, E.B., Martins-Lopes, P., Lopes, C.M., Gaivão, I., Silva, A.M., Guedes-Pinto, H., 2009. A note on regulatory concerns and toxicity assessment in lipid-based delivery systems (LDS). J. Biomed. Nanotechnol. 5, 317–322.
Su, Y., Sinko, P.J., 2006. Drug delivery across the blood–brain barrier: why is it difficult? How to measure and improve it? Expert Opin. Drug Deliv. 3, 419–435.
Tosi, G., Costantino, L., Ruozi, B., Forni, F., Vandelli, M.A., 2008. Polymeric nanoparticles for the drug delivery to the central nervous system. Expert Opin. Drug Deliv. 5, 155–174.
Triplett, M.D., Rathman, J.F., 2009. Optimization of β-carotene loaded solid lipid nanoparticles preparation using a high shear homogenization technique. J. Nanopart. Res. 11, 601–614.
Tröster, S.D., Wallis, K.H., Müller, R.H., Kreuter, J., 1992. Correlation of the surface hydrophobicity of 14C poly(methyl methacrylate) nanoparticles to their body distribution. J. Control. Release 20, 247–260.
Yang, R., Gao, R., Li, F., He, H., Tang, X., 2011. The influence of lipid characteristics on the formation, in vitro release, and in vivo absorption of protein-loaded SLN prepared by the double emulsion process. Drug Dev. Ind. Pharm. 37, 139–148.
Zara, G.P., Bargoni, A., Cavalli, R., Fundarò, A., Vighetto, D., Gasco, M.R., 2002. Pharmacokinetics and tissue distribution of idarubicin-loaded solid lipid nanoparticles after duodenal administration to rats. J. Pharm. Sci. 91, 1324–1333.
Zensi, A., Begley, D., Pontikis, C., Legros, C., Mihoreanu, L., Wagner, S., Büchel, C., von Briesen, H., Kreuter, J., 2009. Albumin nanoparticles targeted with ApoE enter the CNS by transcytosis and are delivered to neurones. J. Control. Release 137, 78–86.